



High-intensity focused ultrasound with large scale spherical phased array for the ablation of deep tumors^{*}

Xiang JI^{§1,2}, Jing-feng BAI^{§1,2}, Guo-feng SHEN^{†‡1,2}, Ya-zhu CHEN^{1,2}

(¹Department of Biomedical Engineering, Shanghai Jiao Tong University, Shanghai 200240, China)

(²Biomedical Instrument Institute, Med-X Research Institute, Shanghai Jiao Tong University, Shanghai 200030, China)

[†]E-mail: shenguofeng@sjtu.edu.cn

Received May 5, 2009; Revision accepted July 22, 2009; Crosschecked Aug. 10, 2009

Abstract: Under some circumstances surgical resection is feasible in a low percentage for the treatment of deep tumors. Nevertheless, high-intensity focused ultrasound (HIFU) is beginning to offer a potential noninvasive alternative to conventional therapies for the treatment of deep tumors. In our previous study, a large scale spherical HIFU-phased array was developed to ablate deep tumors. In the current study, taking into account the required focal depth and maximum acoustic power output, 90 identical circular PZT-8 elements (diameter=1.4 cm and frequency=1 MHz) were mounted on a spherical shell with a radius of curvature of 18 cm and a diameter of 21 cm. With the developed array, computer simulations and ex vivo experiments were carried out. The simulation results theoretically demonstrate the ability of the array to focus and steer in the specified volume (a 2 cm×2 cm×3 cm volume) at the focal depth of 15 to 18 cm. Ex vivo experiment results also verify the capability of the developed array to ablate deep target tissue by either moving single focal point or generating multiple foci simultaneously.

Key words: High-intensity focused ultrasound (HIFU), Spherical phased array, Large scale, Deep tissue ablation

doi:10.1631/jzus.B0920130

Document code: A

CLC number: Q62; Q65; R73

INTRODUCTION

High-intensity focused ultrasound (HIFU) or focused ultrasound surgery (FUS) has been widely used as a noninvasive treatment modality for tumor ablation over the past decade. With HIFU, the ultrasonic beams are focused into the target tissues, and the tissue necrosis is generated by elevating the temperature in the focal region above 60 °C in a short period without damaging the surrounding tissues. As deep tumors to be treated measure up to several centimeters in diameter, treatment with HIFU presents many advantages over other physical therapies (i.e., radiofrequency ablation, laser ablation, and cryoablation) (Kennedy, 2005). Under some circumstances

surgical resection is feasible in a low percentage for the treatment of deep tumors. Nevertheless, HIFU can fulfill the requirements for noninvasive treatment of deep tumors. Ablating solid tumors deep within the body has been achieved using HIFU clinically, aiming at different sites including bone, the liver, the kidney, and the pancreas (Kennedy, 2005).

To date, many studies on the designs of ultrasound phased arrays have been carried out to ablate deep tumors. A large scale 2.5-dimensional (2.5D) phased array has the capability of electronic focusing and beam steering in a wider range of 3D volume. One example of a 2.5D design is a spherical array that used 256 square elements periodically distributed and could ablate the target volume accurately in the liver (N'Djin *et al.*, 2008). Another experimental design is an aperiodic array with 300 circular elements that could avoid the overheating effect caused by the rib (Pernot *et al.*, 2007). Experimental tests have been confirmed that these phased arrays appear safe and

[‡] Corresponding author

[§] The two authors contributed equally to this work

^{*} Project supported by the National Natural Science Foundation of China (No. 30800246) and Shanghai Key Technologies R&D Program of China (No. 09441900500)

effective in the deep tissue ablation. However, the compact element arrangement in these arrays has led to large numbers of elements (>200). Therefore, in these designs each of the elements has to be made small enough to be deployed in the same arrays, or the size of arrays will be enlarged to comprise all the elements. As the element size is inversely proportional to frequency, small element in line with high frequency may lead to the focal depth limitation in tissue ablation. In addition, to support the phased arrays with numerous elements, the ultrasound driving system should add more channels of power amplifiers. Thus, provided that the target focal depth and focal steering range have been achieved, the element number for the array should be minimized. A large scale spherical phased array with less than 100 elements was designed and tested in simulation by our team, allowing enough depth to ablate deep seated tissue (Zhang and Chen, 2007). Such array has not been yet fabricated for use in the experiment. To ablate the deep tissue in the experiment, further modifications on the parameters of the array and element were carried out in this study.

The object of this study is to experimentally confirm the ability of the developed phased array to ablate the target volume in deep tissue. To accomplish this goal, with the required focal depth taken into account, the parameters of the array were first determined in the array design. A large scale 90-element spherical phased array was then constructed using PZT-8 material. Before the experiments, computer simulations were performed to enable the desired focusing modes. Finally, the array was tested in a series of ex vivo experiments on the porcine muscles. The experimental results not only confirm that the developed array can coagulate the target volume in deep-seated tissue, but also indicate that the proposed array may have potential applications in ablating large tumors.

MATERIALS AND METHODS

Array design and construction

Spherical-section phased arrays with large apertures are capable of electronically focusing and steering the beams in a 3D volume with high intensity gain (Ebbini and Cain, 1991). Therefore, such ge-

ometry was chosen for the large scale array. In this study, a large scale array is defined with a 10~20-cm radius of curvature and a 15~25-cm diameter, and the array was designed to ablate target tissue at a focal depth of approximately 15~16 cm. As radius of curvature determines the possible maximum focal depth of the array, the radius of curvature for the array was set at 18 cm. The intensity of the main lobes along with grating lobes is mainly a function of the array f -number and frequency (Daum and Hynynen, 1999a). The f -number was chosen to be <1.0 to minimize the near field heating of a single focus sonication (Daum and Hynynen, 1999b). Moreover, the diameter of the array determines the possible focal range in the cross section. Thus, the diameter of the array was set at 21 cm. A central hole in the array was reserved for an ultrasonic imaging transducer placement in future development. In addition to avoid the cavitation caused by low frequency ultrasound, the increased attenuation of high frequency ultrasound was also taken into consideration. Therefore, the resonance frequency was chosen to be 1.0 MHz.

To minimize the grating lobes, the ratio of the inter-element spacing to the wavelength should be kept as low as possible (Steinberg, 1976). However, the aperture of the array should be also maximized in practice when considering the focal steering range. In addition, in some designs of large scale arrays the compact arrangements of small square elements may lead to large amounts of elements. Thus, a non-compact circular element distribution was employed to control the element number in the array design. Compared with the random element distribution in the arrays (Goss *et al.*, 1996; Gavrilov and Hand, 2000), the elements were designed to be distributed in an annular shape, wherein each ring evenly arranged the elements. The angles between the first elements in every two neighboring rings and X -axis varied (Fig.1). Unequal inter-element spacing was used to compress the grating lobes (Ebbini and Cain, 1991; Goss *et al.*, 1996; Gavrilov and Hand, 2000; Li *et al.*, 2001), wherein the distances between elements in every two neighboring rings varied. In addition, the vertical distances between every two neighboring rings also varied.

The range of element size was first determined by frequency. The individual element dimensions were then optimized to obtain the minimum element

number. The element number was calculated to maximize the spherical surface covered by elements. Meanwhile the ring number was determined to minimize the inter-element spacing in the outer ring. Under the above restricted conditions, the designed spherical array contained an 18-cm radius of curvature and a 21-cm diameter, wherein 90 identical circular elements (diameter=1.4 cm and frequency=1 MHz) were distributed in 6 concentric rings (Fig.1).

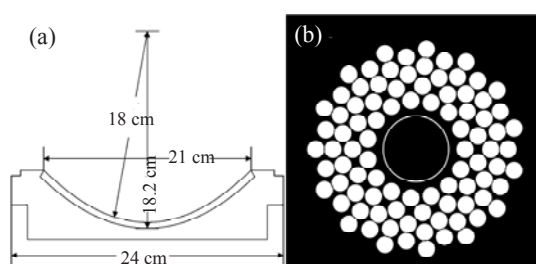


Fig.1 Geometry of the designed array
(a) Side view; (b) Vertical view

Currently the importance of choosing an appropriate piezoceramic material for element is increasing, because it influences both electrical and acoustical properties of the array. PZT-8 material was chosen and cut into 90 planer circular elements. These elements were mounted on a spherical shell to form the complete array. The 90-element array (Shanghai Institute of Ceramics Chinese Academy of Sciences, Shanghai, China) was constructed with an 18-cm radius of curvature and a 21-cm diameter. To place the ultrasonic imaging transducer in the future development, a 5-cm central hole was placed in the spherical shell. Although the array geometry was said to be spherically sectioned, each planer element (1.4 cm in diameter and 0.2 cm thick) was tangent to the spherical shell surface at its center. The matching layers were affixed to the elements with the adhesives poured onto the external surface of the elements. Each element, which was electronically matched to 50 Ω using LC circuit, had its individual independent exciting unit in the ultrasound driving system. On the back of the array, one end of each copper wire with the outside insulator stripped was soldered directly to each element electrode, and the other end was installed on the back of the distributed printed circuit board (PCB). At the front of PCB 90 square connectors were located; therefore, each element was indi-

rectly connected to a 5-m, SJ1563-80 shield coaxial cable. To avoid cross-talk between elements, 90 shield coaxial cables were connected to the ultrasound driving system through a fixed 90-position connecting panel.

Ultrasound driving system

An in-house developed 90-channel ultrasound driving system is used to drive the phased array. The driving system contains the phase signal generator, voltage magnitude controller, and 90 channels of power amplifiers. The phase signal generator can produce 1 MHz square wave signals with the minimum phase resolution of 1.4° . The voltage amplitude controller can generate direct current (DC) signals of 0 to 25 V. The DC signals with the phase signals are input into the power amplifiers, and an alternating current (AC) sine wave signal of 0~110 V can be then delivered to each of the elements via filtering and amplifying components. The total electric power consumption was calculated by summing up the measured electric power consumptions of each channel of the power amplifiers in the experiment. The maximum total electric power consumption was about 1400 W, and the electric power output efficiency of the power amplifiers about was 60%. Thus, the developed array could provide an electric power of up to about 840 W, while the acoustic power contributed by each of the elements was about 6 W.

Simulation

Numerical simulation programs were developed to test the performance of the array, mainly regarding the distribution of acoustic intensity field. One criterion to theoretically assess spherical phased arrays is whether the grating lobes more than 15% of the main lobe are generated when the single focus is shifted along or off the axis (Gavrilov and Hand, 2000). In order to directly synthesize desired focus modes, the array element amplitude and phase distribution were calculated using an inverse method (Ebbini and Cain, 1989). The point source method was employed to model the pressure field as a summation of acoustic point sources (Hutchins *et al.*, 1986). Each circular element was divided into finite tiny areas (ΔA), so small that they can be regarded as point sources. Thus, the total acoustic pressure P at any point (x, y, z) in the field resulted from N elements can be calculated by:

$$P(x, y, z) = j \frac{\rho c k}{2\pi} \sum_{n=1}^N \mu_n \sum_{\text{Surface}} \frac{\Delta A_n e^{-(\alpha + jk)r_n}}{r_n}, \quad (1)$$

where ρ is the density of medium (1060 kg/m³), c the speed of sound (1500 m/s), k the wave number [$2\pi f/c$, where f is the resonance frequency (1 MHz)], α the attenuation coefficient (5.4 Np/(m·MHz)), ΔA_n the area of the corresponding point source on the n th element, r_n the distance between point (x, y, z) and the divided point source on the n th element, and μ_n the n th element's surface velocity as a function of amplitude and phase. The acoustic intensity I of the corresponding point (x, y, z) in the field can be obtained as:

$$I(x, y, z) = \frac{|P(x, y, z)|^2}{2\rho c}. \quad (2)$$

This array was capable of focusing and steering in a 2 cm×2 cm×3 cm cube with a maximum focal depth of about 18 cm. Fig.2 shows the volume in which the foci can be generated and shifted. Attempting to focus out of the volume will lead to a significant increase in grating lobes.

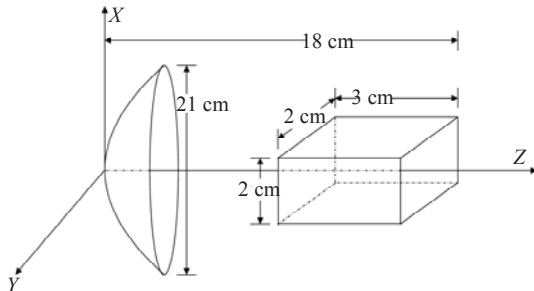


Fig.2 The array was designed to focus and steer with an acceptable grating lobe level, within the cubic volume in front of the spherical transducer

Steering the focal point directly results in the grating lobes, because increasing the shifted distance causes an unpredictable increase in the grating lobe level. The focal points in the X - Y plane and Z -direction were steered in this simulation. For a point focused at (0, 0, 150) mm, the result has given a normalized intensity distribution with a grating lobe level at about -13 dB (Fig.3a). Moving the focal point in the X -direction to (5, 0, 150) mm caused the grating

lobe level to become -12 dB (Fig.3b). Further increase of the steering distance increased the grating lobe level. As shown in Fig.3c, for a focus at (10, 0, 150) mm, the grating lobe level was increased to about -8 dB. Efforts in moving the focal point outside the volume were in vain due to the considerable resulting grating lobes (Fig.2). A focus at (13, 0, 150) mm (off-axis steering distance=13>10 mm) generated the grating lobes with an unacceptable maximum level of -5 dB (Fig.3d). The focal steering in the Y -direction had similar results due to the symmetry of the X - Y plane. For the Z -direction movement, the points focused at (0, 0, 140), (0, 0, 150), (0, 0, 160), (0, 0, 170), (0, 0, 180) and (0, 0, 190) mm in sequence, Figs.4a-4f demonstrate the corresponding results as a mesh. All of the grating lobe levels resulting from focusing in the volume were reduced from -9 to -10 dB (Fig.2), and were under control. However, the grating lobe level was increased to -6 dB so long as focused at (0, 0, 140) or (0, 0, 190) mm outside the volume (Figs.4a and 4f). The above simulation results show that the designed array can steer in a large volume (2 cm×2 cm×3 cm) as well as a large focal depth (at least 15 cm) with an acceptable grating lobe level.

Increase in necrosis area can be achieved by generating multiple foci simultaneously. Two focal points were generated at ($\pm 10, 0, 150$) mm at the same time, and the normalized intensity distributions in the X - Y and X - Z planes are shown in Fig.5. The simulations demonstrated that the designed array can not only steer in a 3D volume but also simultaneously generate multiple focal points with the controllable grating lobe level.

Ex vivo experiments

In the experiment, the developed array was installed at the bottom of a polymethyl cylindrical tank. The tank, 32 cm in height and 24 cm in diameter, was filled with degassed and deionized water. Fresh porcine muscles were selected, cut into cubic units, and then laid on a clean plate until reaching the room temperature. The cubic unit was placed on an acoustic transmission membrane in the tank and a distance of 11 cm was kept between the bottom of the array and the membrane (Fig.6). Furthermore, the distance between the focal plane and the bottom of the array was fixed at 15 cm in the experiments.

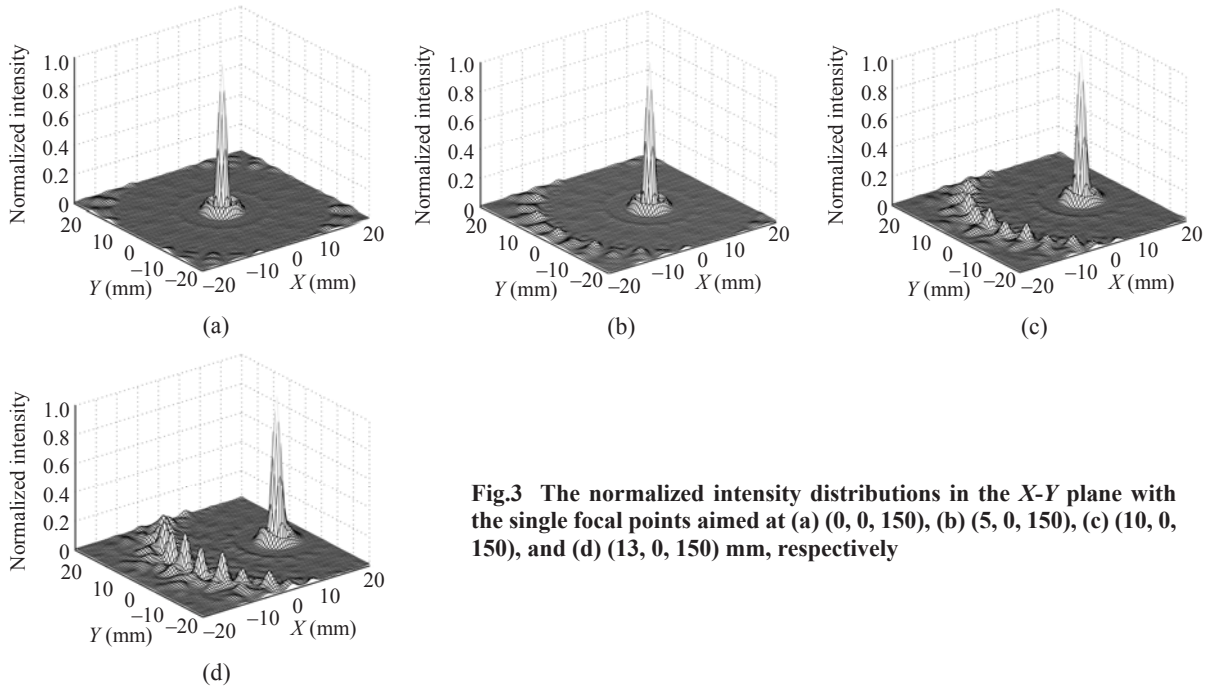


Fig.3 The normalized intensity distributions in the X-Y plane with the single focal points aimed at (a) (0, 0, 150), (b) (5, 0, 150), (c) (10, 0, 150), and (d) (13, 0, 150) mm, respectively

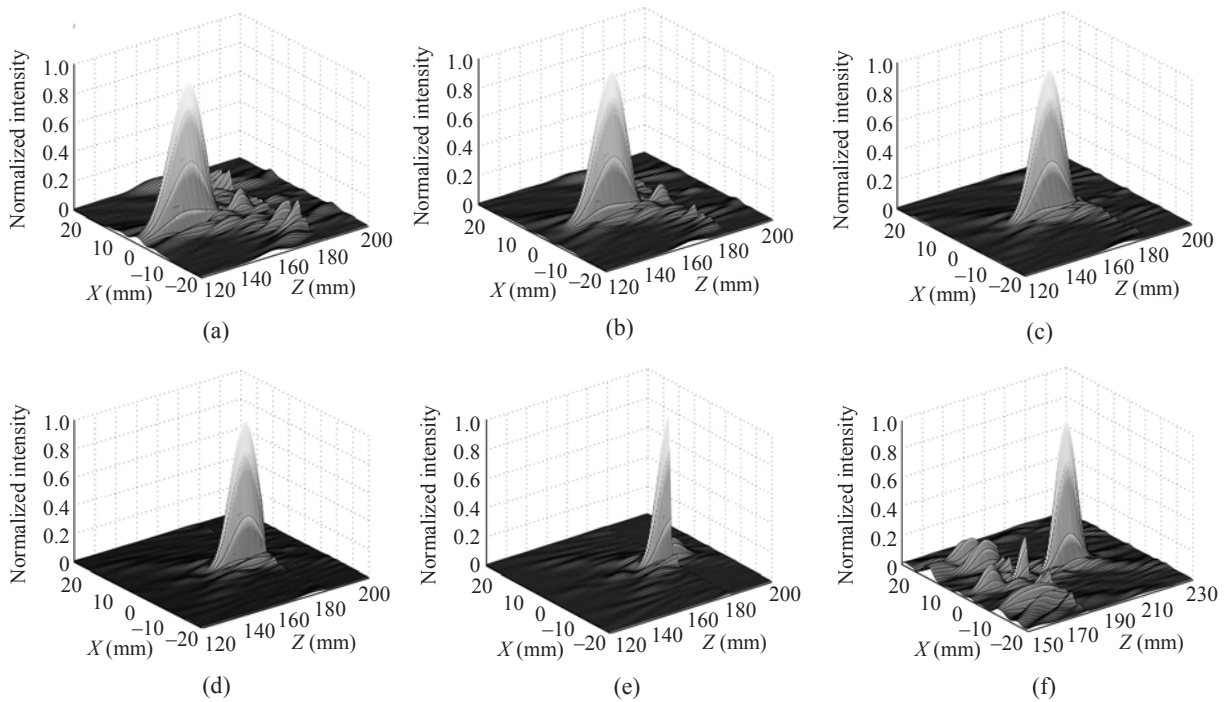


Fig.4 The normalized intensity distributions in the X-Z plane with the single focal points aimed at (a) (0, 0, 140), (b) (0, 0, 150), (c) (0, 0, 160), (d) (0, 0, 170), (e) (0, 0, 180), and (f) (0, 0, 190) mm, respectively

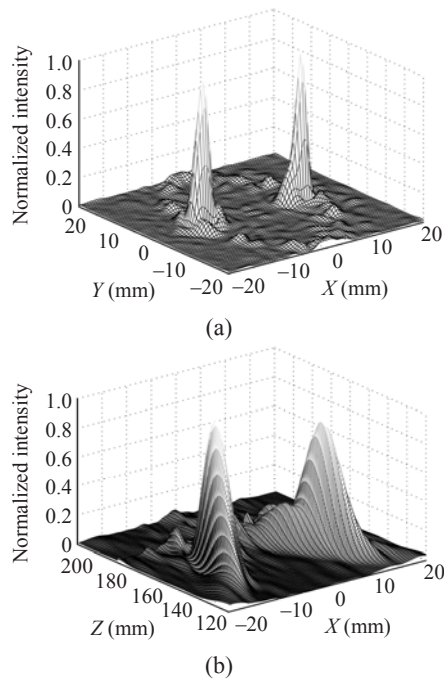


Fig.5 The normalized intensity distributions for two points focused at $(\pm 10, 0, 150)$ mm simultaneously in (a) the X - Y plane and (b) the X - Z plane

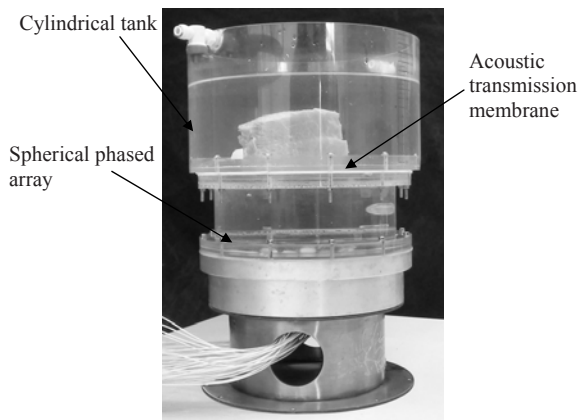


Fig.6 Experimental set-up prototype

With the following three experiments, the ultrasound driving system provided the electric power consumption of about 756 W, while the acoustic power was about 300 W. In the first experiment, the heating periods were 17 s for both on-axis and off-axis focusings. In addition, one focal point off axis was 1 cm from another focal point on axis. For the second experiment, 17 on-axis and off-axis points with 2-mm adjacent spacing were focused sequentially to produce an H-shaped lesion. In the final experiment, two points focused simultaneously with

2-cm spacing were heated for 50 s. Following the sonication, the porcine muscles were sliced through the focal plane parallel to the X - Y plane, and the lesions were then measured and photographed.

RESULTS AND DISCUSSION

To verify the capability of this array to ablate deep tissue (focal depth > 10 cm), ex vivo experiments were performed on porcine muscles. In the first experiment, two positions at $(0, 0, 150)$ and $(10, 0, 150)$ mm were sequentially focused. Each of the foci was heated for 17 s, resulting two separate lesions with different sizes. Fig.7 shows a photograph of the two lesions, 2 and 5 mm in diameter, respectively, which corresponded to the heating sequence. Another experiment was performed to test the feasibility of generating shaped lesions as desired. Seventeen on-axis and off-axis points, which constituted an H-like shape, were focused in sequence. The focal points were in the $z = 150$ mm plane and the total heating time was increased to 53.6 s (Fig.8b). The dot lesions, which were observed to be about 2 mm in diameter, almost partially overlapped the adjacent ones to form the H-shaped lesion. As shown in the simulations (Fig.5), the array was theoretically capable to simultaneously generate multiple foci. To confirm it experimentally, two separate lesions at $(\pm 10, 0, 150)$ mm (Fig.9), 5 and 6 mm in diameter, respectively, simultaneously resulted from a 50-s heating period.

Large scale spherical phased arrays provide a choice of transducer for HIFU in deep tissue ablation due to their large focal depth and steering range. One persuasive reason for using the large scale spherical

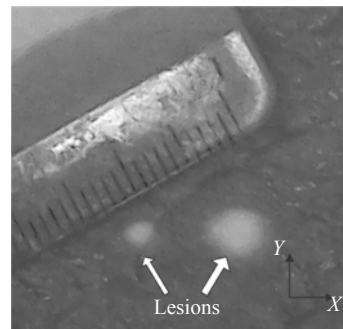


Fig.7 Lesions generated by single focal points aimed at $(0, 0, 150)$ and $(10, 0, 150)$ mm in sequence for 17 s

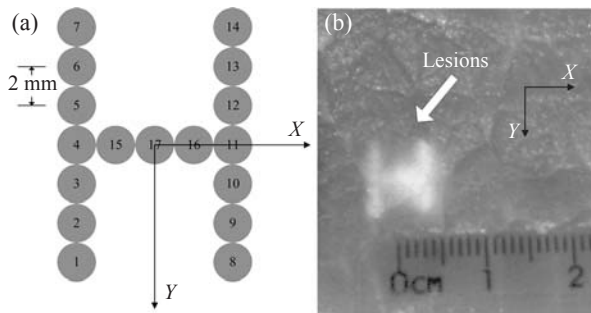


Fig.8 (a) Schematic illustration of single focusing scanning protocol. The number indicates sonication sequence; (b) Ex vivo experimental result of lesions created with on- and off-axis focusing in the $Z=150$ mm plane for various heating time points, and was scanned with the protocol defined in (a)

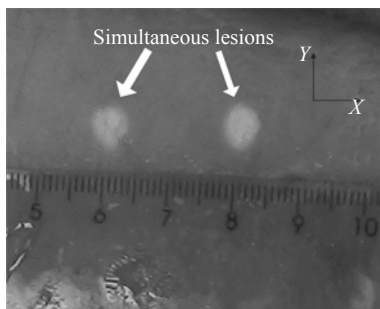


Fig.9 Lesions resulted from two points focused at $(\pm 10, 0, 150)$ mm simultaneously heated for 50 s

phased array with focused ultrasound is that a large focal depth (>10 cm) can be easily achieved. Meanwhile, the element number has the room to be diminished at the cost of narrowing the steering range. In the design of the similar arrays to ablate deep tumors, the radius of curvature should be 2~3 cm larger than the required focal depth. In addition, the size of element should be also taken into consideration. Choosing the unequal inter-element spacing design ensures that controllable focusing modes are generated on the basis of weakening the near field heating.

Previously many focused ultrasound transducers have been developed for deep-seated tissue ablation.

However, some single-element focused transducers require mechanical movements to reposition the focus; planar phased arrays are capable of focusing in a fixed angle. In addition, some spherical arrays (Filonenko *et al.*, 2004; Lu *et al.*, 2008; N'Djin *et al.*, 2008; Pernot *et al.*, 2007), which are similar to the proposed array, have demonstrated good performance in beam focusing and steering. They have consisted of over 200 elements with small size, which may cause the increase in the cost in terms of manufacture complexity and individual power amplifier channels. This study provides another design for large scale spherical arrays. The designed array can be not only flexibly controlled to steer the focus throughout the target volume with an acceptable level of grating lobes, but also easily constructed with a high performance price ratio. Thus, this 90-element spherical phased array with a large scale was designed and constructed. Table 1 shows the comparative parameters of these arrays and the proposed array. As the production and mounting of elements were implemented with a simple process and a low cost, further improvement of the proposed array seems feasible due to the development of new focused transducer materials. In the array construction, piezocomposite technology integrates elements closely with the surface of the spherical shell. A multi-layer material may be used to improve the breakdown voltage of elements, and therefore make it easier to increase electric power input of the array.

The proposed array may also ablate large tumors. As shown in Fig.2, the volume that the array can necrose depends on its steering range. Provided that the center of the target volume is 16.5 cm deep, this array is able to ablate a volume of at least 2 cm \times 2 cm \times 3 cm without mechanically moving the array. When treating an irregular large tumor, the tumor needs to be cut into several layers, each of which is 2 mm thick and parallel to the X - Y plane. Two methods can be

Table 1 Comparative parameters of the four phased arrays and the proposed array

Array	Element number	Radius of curvature (cm)	Diameter (cm)	f -number	Size of element	Wavelength (cm)
I ^a	256	12	13	0.92	0.5 ^e	0.10
II ^b	256	11	14	0.78	0.49 ^f	0.14
III ^c	256	7	7	1	0.13 ^g	0.05
IV ^d	300	NA	NA	NA	0.8 ^e	0.15
Proposed array	90	18	21	0.86	1.4 ^e	0.15

^a Filonenko *et al.*, 2004; ^b Lu *et al.*, 2008; ^c N'Djin *et al.*, 2008; ^d Pernot *et al.*, 2007. ^e Diameter (cm); ^f Projection area (cm²); ^g Area (cm²)

used. One is the single focal point scanning. Every layer is divided into small points and the sizes of these points lie with the size of a single lesion and heating time. Heated for 17 s, the lesion was found to be a rice-shape with a 2-mm diameter (Fig.7). Therefore, the number of points is determined based on a single 17-s heating, and single focusing is scanned throughout these points. Taking one of these points as a start point, a single point is focused there and then moved several times to scan throughout all the points. An issue concerning this method is uncontrolled residual heat deposition of focal points, which can be avoided by setting adequately long distance between two focal points in sequence and giving enough time to the post-focal points to cool down. Another method to ablate large tumors is to use simultaneous multi-point focusing, and the heating process is the same as single focusing scanning. This method increases total necrosis zone per sonication, but the drawback behind it is more electric power required to keep the focal intensity.

As the effective focal depth for the proposed array ranged from 15 to 18 cm, focusing beyond this distance will cause an undesired heating resulting from the significantly increasing grating lobes. This limits the array if the target volume extends outside the 3-cm distance. The possible maximum steering in the plane parallel to the X - Y plane is $2\text{ cm}\times 2\text{ cm}$. However, ultra-large tumors generally reach a diameter of over 5 cm, which results in another limitation when ablating ultra-large tumors.

Similar to deep tissue ablation, the solid tumors deep within the liver are currently treated clinically by mechanically moving single-element focused transducers to steer focal points (Kennedy *et al.*, 2004). In addition, magnetic resonance imaging (MRI) was employed for guidance and feedback control in the treatment (Diederich *et al.*, 2004). The treatment has been shown to be effective, nonetheless the heating procedure lasts a considerably long period due to the mechanical scanning strategy. With closely located targets ablated, neighboring exposure accumulations result in heat deposition. Hence, cooling time between adjacent exposures is needed to dissipate heat, and as such this would inevitably prolong the procedure. With phased arrays, flexible focusing modes can be formed to ablate non-neighboring regions in the tumor so that there is enough time for the

post-focusing to cool down. A treatment planning is required to be made based on scanning path optimization in the entire tumor region. The target volume can be necrosed throughout distant and non-adjacent focal points to reduce post-focusing thermal deposition in an acceptable period.

CONCLUSION

We verified the capability of the proposed array in both simulations and *ex vivo* experiments and found that the developed array can effectively ablate the deep tissue by generating single or multiple focal points. Such a large scale spherical array can steer the focus in a $2\text{ cm}\times 2\text{ cm}\times 3\text{ cm}$ volume with an effective focal depth ranging from 15 to 18 cm. The array design based on large scale spherical geometry has experimentally proved its effectiveness in ablating deep tissues. In conjunction with the annular-shaped element distribution, the arrangement of the same element number in each ring can provide larger scales of geometry but relatively small element number. This study suggests that the similarly designed arrays are suitable for the deep tissue ablation.

References

- Daum, D.R., Hynynen, K., 1999a. A 256-element ultrasonic phased array system for the treatment of large volumes of deep seated tissue. *IEEE Trans. Ultrason. Ferroelectr. Freq. Control*, **46**(5):1254-1268. [doi:10.1109/58.796130]
- Daum, D.R., Hynynen, K., 1999b. Theoretical design of a spherically sectioned phased array for ultrasound surgery of the liver. *Eur. J. Ultrasound*, **9**(1):61-69. [doi:10.1016/S0929-8266(99)00006-3]
- Diederich, C.J., Stafford, R.J., Nau, W.H., Burdette, E.C., Price, R.E., Hazle, J.D., 2004. Transurethral ultrasound applicators with directional heating patterns for prostate thermal therapy: in vivo evaluation using magnetic resonance thermometry. *Med. Phys.*, **31**(2):405-413. [doi:10.1118/1.1639959]
- Ebbini, E.S., Cain, C.A., 1989. Multiple-focus ultrasound phased-array pattern synthesis: optimal driving-signal distributions for hyperthermia. *IEEE Trans. Ultrason. Ferroelectr. Freq. Control*, **36**(5):540-548. [doi:10.1109/58.31798]
- Ebbini, E.S., Cain, C.A., 1991. A spherical-section ultrasound phased array applicator for deep localized hyperthermia. *IEEE Trans. Biomed. Eng.*, **38**(7):634-643. [doi:10.1109/10.83562]
- Filonenko, E.A., Gavrilov, L.R., Khokhlova, V.A., Hand, J.W., 2004. Heating of biological tissues by two-dimensional

- phased arrays with random and regular element distributions. *Acoust. Phys.*, **50**(2):222-231. [doi:10.1134/1.1675879]
- Gavrilov, L.R., Hand, J.W., 2000. A theoretical assessment of the relative performance of spherical phased arrays for ultrasound surgery. *IEEE Trans. Ultrason. Ferroelectr. Freq. Control*, **47**(1):125-139. [doi:10.1109/58.818755]
- Goss, S.A., Frizzell, L.A., Kouzmanoff, J.T., Barich, J.M., Yang, J.M., 1996. Sparse random ultrasound phased array for focal surgery. *IEEE Trans. Ultrason. Ferroelectr. Freq. Control*, **43**(6):1111-1121. [doi:10.1109/58.542054]
- Hutchins, D.A., Mair, H.D., Puhach, P.A., Osei, A.J., 1986. Continuous-wave pressure fields of ultrasonic transducers. *J. Acoust. Soc. Am.*, **80**(1):1-12. [doi:10.1121/1.394164]
- Kennedy, J.E., 2005. High-intensity focused ultrasound in the treatment of solid tumours. *Nat. Rev. Cancer*, **5**(4):321-327. [doi:10.1038/nrc1591]
- Kennedy, J.E., Wu, F., ter Haar, G.R., Gleeson, F.V., Phillips, R.R., Middleton, M.R., Cranston, D., 2004. High-intensity focused ultrasound for the treatment of liver tumours. *Ultrasonics*, **42**(1-9):931-935. [doi:10.1016/j.ultras.2004.01.089]
- Li, G.W., Xiong, B., Chen, Y.Z., 2001. Ultrasound spherical phased-array and the effect of phased and magnitude precision. *Shanghai Jiaotong Daxue Xuebao*, **35**(9):1412-1414 (in Chinese).
- Lu, M.Z., Wang, X.D., Wan, M.X., Feng, Y., Xu, F., Zhong, H., Tan, J.W., 2008. Image-guided 256-element phased-array focused ultrasound surgery. *IEEE Eng. Med. Biol. Mag.*, **27**(5):84-90. [doi:10.1109/MEMB.2008.923952]
- N'Djin, W.A., Melodelima, D., Parmentier, H., Chesnais, S., Rivoire, M., Chapelon, J.Y., 2008. Utility of a tumor-mimic model for the evaluation of the accuracy of HIFU treatments. Results of in vitro experiments in the liver. *Ultrasound Med. Biol.*, **34**(12):1934-1943. [doi:10.1016/j.ultrasmedbio.2008.04.012]
- Pernot, M., Aubry, J.F., Tanter, M., Marquet, F., Montaldo, G., Boch, A.L., Kujas, M., Seilhean, D., Fink, M., 2007. High Power Phased Array Prototype for Clinical High Intensity Focused Ultrasound: Applications to Transcostal and Transcranial Therapy. 29th Annual International IEEE EMBS Conference, Lyon, France. IEEE, USA, p.234-237. [doi:10.1109/EMBS.2007.4352266]
- Steinberg, B.D., 1976. Principles of Aperture and Array System Design. Wiley, New York.
- Zhang, C.X., Chen, Y.Z., 2007. Investigation of a spherical-section ultrasound phased array for hepatic ablation. *J. Zhejiang Univ. Sci. A*, **8**(8):1237-1245. [doi:10.1631/jzus.2007.A1237]